Characterization of surface dielectric barrier discharge influenced by intermediate frequency for ozone production

Characterization of surface dielectric barrier discharge influenced by intermediate frequency for ozone production

Ayman A. Abdelaziz[1,2], Tatsuo Ishijima[3], Takafumi Seto[4], Naoki Osawa[5], Hassan Wedaa[6], Yoshio Otani[4]

[1] Physics Department, Faculty of Science, Assiut University, Assiut, Egypt

[2] Centre for Water Advanced Technologies and Environmental Research, College of engineering, Swansea University, Swansea, UK

[3] Research Center for Sustainable Energy and Technology, Kanazawa University, Kakuma-machi, Kanazawa, Japan

[4] School of Natural System, Kanazawa University, Kakuma-machi, Kanazawa, Japan

[5] Center for Electric, Optic and Energy Applications, Department of Electrical and Electronic Engineering, Kanazawa Institute of Technology, Kanazawa, Japan

[6] Electrical Engineering Department, Assiut University, Assiut, Egypt

Corresponding author: Ayman A. Abdelaziz, Tel.: +441792602303,

E-mail: a.abdelaziz@science.au.edu.eg and a.abdelaziz@swansea.ac.uk

Abstract

The aim of this study is to investigate the effect of the intermediate frequency (1–10 kHz) of the sinusoidal driving voltage on the characteristics of a developed surface dielectric barrier discharge (SDBD)-based reactor having spikes on its discharge electrode. Moreover, its influence on the production of ozone and nitrogen oxide byproducts is evaluated. The results show that SDBD is operated in the filamentary mode at all the frequencies. Nevertheless, the pulses of the discharge current at high frequencies are much denser and have higher amplitudes than those at low frequencies. The analysis of the power consumed in the reactor shows that a small portion of the input power is dissipated in the dielectric material of SDBD source, whereas the major part of the power is consumed in the plasma discharge. The results of the ozone production show that higher frequencies have a slightly adverse effect on the ozone production at relatively high energy density values, where the ozone concentration is slightly decreased when the frequency is increased at the same energy density. The temperature of the discharge channels and gas is not a crucial factor for the decomposition of ozone in this reactor, while the results of the measurements of nitrogen oxides characteristics

indicate that the formation of NO and NO_2 has a significant adverse effect on the production efficiency of ozone due to their oxidation to another nitrogen oxides and their catalytic effect.

1. Introduction

Over the past two decades, nonthermal plasma has been employed as a promising technology for versatile applications in environmental and biological fields [1–4]. The main feature of nonthermal plasma is the generation of reactive species such as O, O_3, and OH, which are capable of decomposing organic pollutants and killing microorganisms at the atmospheric pressure and temperature. A variety of techniques have been used to generate nonthermal plasma for environmental and biological applications. Among these techniques, surface dielectric barrier discharge (SDBD), which is sometimes called surface microdischarge (SMD), attracts significant attention in different applications. It is applied effectively in the ion production process for the aerodynamic flow control [5] and charging aerosols [6, 7]. It is also used as a plasma-based chemical reactor in many environmental applications, such as ozone production [8–10], NO_x conversion [11], decomposition of VOCs [12, 13], inactivation of microorganisms, and killing bacteria [14–17]. The reasons for growing the interest in SDBD and making it more efficient than conventional dielectric barrier discharge (DBD), wherein the plasma is generated in the volume between the discharge and the grounded electrodes, could be as follows: (1) the reduction of the applied voltage and the increase in the power efficiency [18]; (2) the availability of the free space over the plasma zone that allows the ozone to accumulate without destructing it by a high temperature of the plasma channels or the collisions with reactive species in the plasma zone, [19]; (3) high energy efficiency to produce reactive species, which exceeds that of volume DBD [9, 20]; and (4) operation in ambient air without requiring a noble gas admixture [21].

Practical applications of SDBD, such as degradation of organic pollutants and inactivation of microorganisms, have recently been discussed for water purification [22–25]. Since the plasma of SDBD is generated in a thin layer along the dielectric surface, the drawback of SDBD for water treatment is that it does not reach the treated water. This results in a steep decrease of the concentration of short-lifetime reactive species with high oxidation potentials, such as OH and O radicals, in the water. Therefore, ozone is the most important reactive species generated in the SDBD configuration for environmental applications, especially for water treatment [11]. This is due to its high oxidization ability and its long lifetime, which allow it to attack pollutant molecules near and far away from the plasma zone. Ozone can penetrate the water surface and decompose pollutants through its direct reaction with pollutant molecules or through its indirect effect by its conversion to a shorter-lived aqueous phase species such as a hydroxyl radical and superoxide [26]. However, the production of ozone in air using SDBD is accompanied with the production of nitrogen oxide species such as NO, NO_2, N_2O, and N_2O_5. These species, especially NO_x, can be dissolved in the treated water to produce nitrate (NO_3^-) and nitrite (NO_2^-), which play a major role in water acidification [22, 27] that is important for biological applications [28, 29]. On the other hand, these nitrogen oxide byproducts have an adverse effect on the gas treatment process due to their reactions with pollutants and intermediate byproducts resulting in the production of more toxic compounds. Hence, before using SDBD in any application, the trends of the ozone production and the generation of nitrogen oxides should be characterized. Few works on the ozone production using different SDBD sources under different conditions exist [11, 30–34].

Apparently, the ozone concentration and its byproducts are correlated to the energy consumed in the reactor, which mainly depends on the electrical parameters of the plasma source, such as the applied voltage and frequency.

In this paper, we focus on the details of the effect of the intermediate frequency on the microdischarge characteristics of SDBD and on the power consumption. Moreover, the SDBD performance influenced by the driven frequency is evaluated for the ozone production. To clarify the efficiency of the reactor for the ozone production, the nitrogen-excited species, nitrogen oxides, and gas temperature are measured. The SDBD characteristics as well as the measurements of ozone and nitrogen oxides are carried out in dry air at the atmospheric pressure inside an enclosed chamber.

Although the present article focuses on the generation of ozone for environmental applications, it is useful for the fields of the aerodynamic flow control and for charging the aerosol process where ozone is considered as an unfavorable product in the ion production process [35].

2. Experimental details

Figure 1(a) shows the schematics of the experimental setup used in the present study. The reactor consists of a glass tube with an inner diameter of 24 mm and a length of 220 mm containing an SDBD source. As shown in figures 1(b) and 1(c), the SDBD source consists of two stainless steel electrodes formed on both sides of a dielectric plate, which is a mica sheet with a thickness of 0.14 mm, width of 6 mm, and length of 188 mm, using photo-etching thin films. Each electrode has a length of 165 mm and a thickness of 50 µm. The upper discharge electrode with spikes spaced at 6 mm intervals has a width of 0.1 mm. The spikes on the discharge electrode can intensify the electric field and thus, plasma discharge [36]. Another electrode with a width of 0.5 mm is covered using a dielectric layer of a polyamide tape with a thickness of 60 µm and connected to the ground. The driving signal is generated using a function generator (Agilent 33521A) and sent to a high-voltage amplifier (Matsusada HEOPT-5B20).

The applied voltage was measured using a high-voltage probe (Tektronix P5210), which was connected to a digital oscilloscope (Tektronix DPO 4032, bandwidth: 350 MHz, 2.5 GS/s, 1 Mpts/CH). The current through the SDBD source was measured using a Pearson current monitor (model 2877, rise time: 2 ns, 1 V/A, bandwidth 300 Hz–200 MHz) and displayed using the digital oscilloscope.
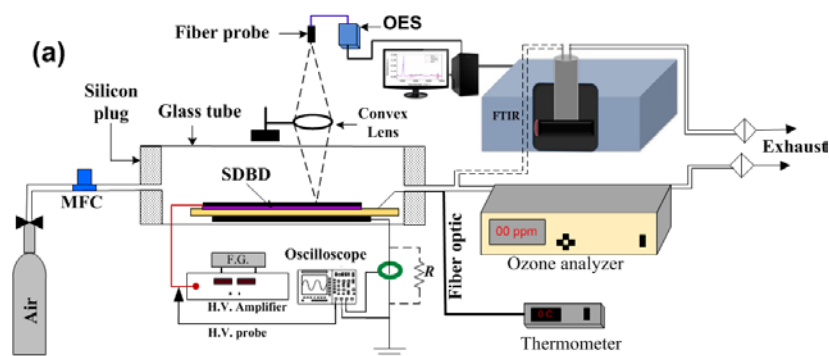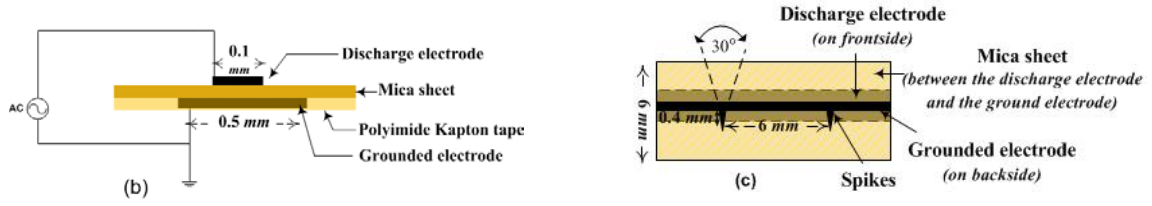
Figure 1 *(a) Schematics of the experimental setup, (b) side view of the SDBD source, and (c) upper view of the SDBD source.*

The ozone production of SDBD was measured at the outlet of the reactor using a UV ozone monitor (Ebara Jitsugyo Co. LTD, EG-3000B/01). The measurements of the ozone concentration were recorded for a given applied voltage and frequency after 2 min from the discharge ignition when the discharge was stable and the steady-state ozone levels were indicated by the O_3 analyzer.

The results of the ozone production are presented as a function of the energy density, which is defined as the energy per unit volume of gas consumed by the discharge reactor and changed with the input power to the reactor. The energy density can be expressed using the following equation:

$$E_d = \frac{60\,P_d}{Q} \tag{1}$$

where E_d, P_d, and Q are the energy density (J/L), discharge power (W), and gas flow rate (L/min), respectively. The energy density is changed with the applied voltage, when the frequency is fixed. In this work, flow rate Q of inlet dry air before entering the reactor was set using a mass flow controller at 2.05 L/min, which makes the working air residence inside the reactor for 2.9 s. The temperature and the pressure were 23 $^\circ$C and 1 atm, respectively. Discharge power P_d, which was the power consumed in the reactor, was calculated based on the time integration of the product of the voltage and current waveforms over one cycle using the following equation:

$$P_d = f \int_0^\tau V(t) \cdot I(t)\,dt \tag{2}$$

where τ and f are the period and driven frequency, respectively. $V(t)$ and $I(t)$ are the instantaneous values of the applied voltage and current, respectively. Current $I(t)$ is measured using two different techniques: a current monitor technique, when the Pearson current monitor is used to measure the current, and a shunt resistor technique. In the latter, a 10 kΩ resistor is connected in series with the reactor (between the grounded electrode and the ground) [36−38], and the current is calculated from the voltage drop across the shunt resistor using Ohm's law. The voltage used for the calculation of the power in equation (1) is the applied voltage that is delivered from the amplifier in the case of the current monitor technique, and it is the voltage across the reactor, which is determined by subtracting the voltage across the resistance from the applied voltage, in the case of the shunt resistor technique. Although the powers calculated using the two different techniques were almost equal, the pulses of the measured current were clearer in the case of the current monitor

4

technique, as shown in figure 2. This is due to its sensitivity to the measurements of low-rise time current pulses. Therefore, in this work, the presented current waveform was measured using the current monitor technique.

The power values used in this study were the average of the three power values corresponding to the three measurements of the current–voltage waveform. The error bars shown in the figures are the 90% confidence interval for the calculated average.

The energy yield (the production yield of ozone) (g/kWh) is defined as an amount of produced ozone per unit input energy and calculated as follows:

$$\eta = 60\ Q\ N\left(\frac{M}{22.4}\right)\left(\frac{10^{-3}}{P_d}\right) = 60\ Q\ N\left(\frac{48}{22.4}\right)\left(\frac{10^{-3}}{P_d}\right) = \frac{48 \times 3.6\ Q\ N}{22.4 \times 60\ P_d}$$

$$\eta = 7.7143\ \frac{N}{E_d} \tag{3}$$

where N and M are the ozone concentration (ppm) and the molecular weight of ozone (48 g/mole), respectively. This equation is based on the fact that one mole of a gas occupies a volume of 22.4 L at a temperature of $0\ ^\circ$C and a pressure of 1 atm.

Nitrogen byproducts including N_2O and NO_2 were measured using a Fourier transform infrared spectrometer (FTIR) (Shimadzu, IRAffinity-1) equipped with a gas cell having a path length of 3 m (Gemini Scientific Instruments, MARS-0.2L/3M). The reactor is connected to the FTIR using a silicon tube with an inner diameter 4-mm and a length 70-mm, which makes the reactive species take 0.26 s to arrive at the gas cell of the FTIR.

The temperature of the dielectric material of the SDBD source was measured by inserting a fiber optic thermometer (Anritsu meter Co. LTD, AMOTH FL-2000) inside the reactor for the direct contact with the mica sheet.
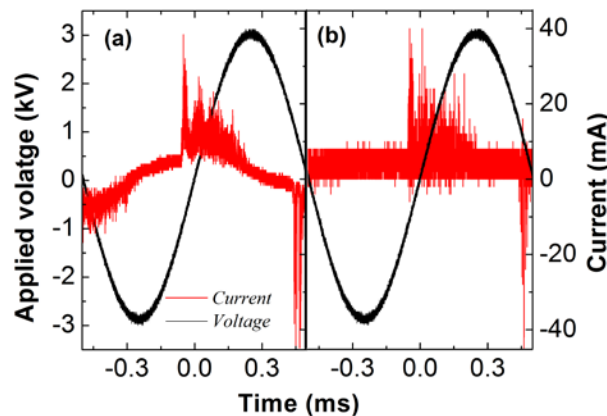

Figure 2 *Current–voltage waveforms of the SDBD at an applied peak-to-peak voltage of 6 kV and at a frequency of 1 kHz measured using (a) current-shunt technique and (b) current monitor technique.*

3. Results and discussion

3.1. Characteristics of the discharge current of SDBD

Typical waveforms of the AC voltage applied to the SDBD reactor and the associated discharge current at frequencies of 1 and 10 kHz as well as constant applied voltage $Vpp = 6$ kV are shown in figure 3.
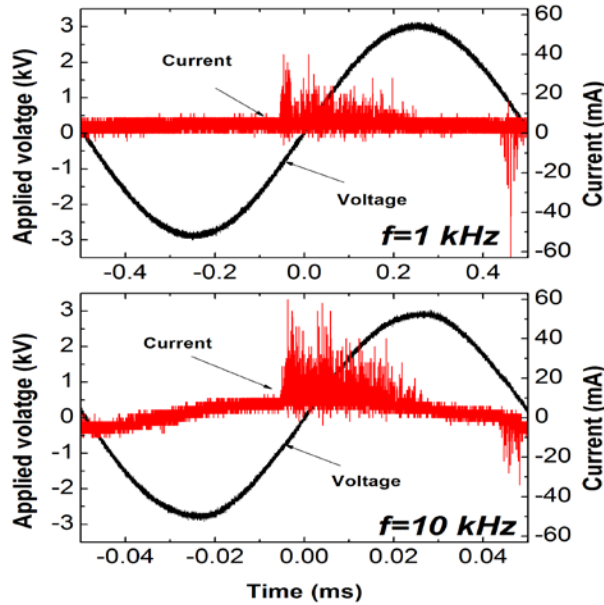

Figure 3 *Waveforms of the voltage applied to the SDBD reactor and the associated discharge current at a peak-to-peak voltage of 6 kV and at frequencies of 1 and 10 kHz.*

The current waveforms at both frequencies of 1 and 10 kHz are mainly composed of the capacitive current and the discharge current, as shown in figure 3. The capacitive current has a sine waveform with a phase shift of $90°$ from the applied voltage waveform. The discharge current appears in the form of pulses superimposed on the capacitive current at the positive and negative halve cycles of the applied voltage. This indicates that discharge is ignited in the SDBD reactor in the form of filamentary streamers at both frequencies of 1 and 10 kHz. The formation and behavior of the streamers in SDBD is explained in detail in [36] for a similar reactor operated at a frequency of 1 kHz, which also can be applied for those at a higher frequency of 10 kHz. Although the modes of SDBD are the same at both frequencies, some differences in the discharge current occur as shown in figure 3, where the pulses of the discharge current at a frequency of 10 kHz are much denser and longer than those at a frequency of 1 kHz. This can be caused by the accumulated charges of the filaments over the dielectric material from the preceding half cycle of the applied voltage, which enhances the electric field and subsequently the discharge in the next half cycle of the applied voltage. Because the time between the two proceeding half cycles decreases when the frequency is increased, the effect of the accumulated charges of the preceding half cycle on the discharge at the next half cycle is significant. Thus, the pulses of the discharge current at a high

6

frequency are much denser and have higher amplitudes than those in case of a low frequency at the same applied voltage, as demonstrated in figure 3. This can also be due to a higher slope of the applied voltage at a high frequency than that at a low frequency, as explained using the optical measurements conducted by Dong et al. [39] and the numerical calculations performed by Boeuf et al. [40]. Therefore, it can be assumed that the frequency change in the SDBD reactor leads to changing not only the repetition of the discharge cycles at a certain time but also the discharge current per voltage cycle.

It is worth to mention that the onset voltage of the discharge did not change significantly with the frequency: it decreased from 2.7 kV to 2.4 kV when the frequency was increased from 1 kHz to 10 kHz, respectively.

Figure 4 shows the photos of the SDBD at different frequencies (1, 5, and 10 kHz) and at an applied peak-to-peak voltage of 6 kV. Bright microdischarge filaments are distributed around the discharge electrode, and the brightness increases with the frequency due to recording more plasma events at high frequency at the same time, where the exposure time of recording these photos are same. Moreover, the photos show that the discharge starts from the edge of the discharge electrode as jets spread over the mica sheet and moves to the edge of the ground electrode. These photos confirm the aforementioned description of the filamentary mode of SDBD in the investigated frequency range of 1–10 kHz.
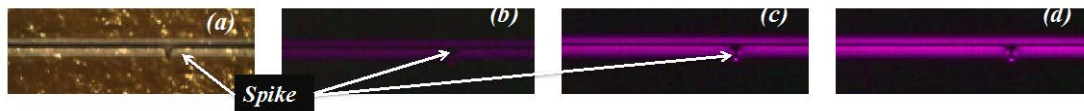

Figure 4 *Photos of the SDBD source (obtained at the fixed exposure time and shutter speed) (a) without discharge at constant voltage V*pp *= 6 kV and with the discharge ((b) f = 1 kHz, (c) f = 5 kHz, and (d) f = 10 kHz).*

3.2. Energy density, optical emission, and temperature

Figure 5 shows the relation between the energy density and the driven frequency of the applied voltage at various peak-to-peak voltages applied to the SDBD reactor. As can be seen, the energy density increases with either the applied voltage or frequency linearly. The energy density increased from 20 J/L at a voltage of 3 kV to 80 J/L at a voltage of 6 kV at the same frequency of 10 kHz, and it increased from 8 J/L at a frequency of 1 kHz to 80 J/L at a frequency of 10 kHz at Vpp = 6 kV.
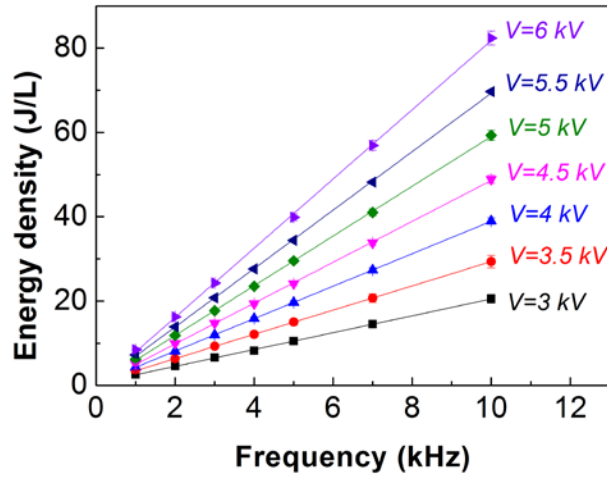
Figure 5 *Energy density in the SDBD as a function of the frequency at different applied peak-to-peak voltages.*

The linear increase of the energy density with the frequency can be explained using the aforementioned description of the current–voltage characteristics, where the discharge at a high frequency is much higher and denser than that at a low frequency despite a short period of the discharge at a high frequency. Therefore, the total energies consumed at one period at high and low frequencies are equal. Thus, the energy density increased with the frequency linearly, i.e., the total power consumed at one period is independent of the driven frequency in our experimental range. The linear correlation between the driven frequency and the energy density obtained in this work is similar to that obtained in [39].

However, figure 5 demonstrates the total energy consumption in the reactor and not the energy consumed by the plasma discharge only. Figure 6 illustrates the distribution of the deposited energy in the plasma reactor for the ozone production.
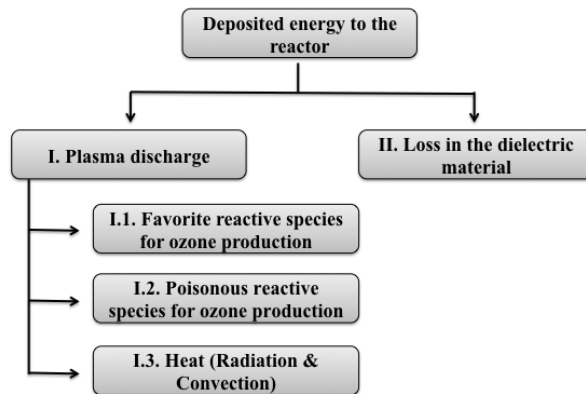

Figure 6 *Diagram of the distribution of the deposited energy in the SDBD.*

A part of the deposited energy is used to generate plasma, which is used to produce reactive species and consumed as heat in the system. Another part of the deposited energy is lost in the dielectric material of the SDBD source. Therefore, the energy consumed in the plasma

8

discharge and the energy dissipated in the dielectric material should be evaluated to clarify the reactor performance to generate reactive species. Since the average power is directly proportional to the energy, the estimation of the discharge power conceives of the energy consumed in the plasma discharge.

The power loss in the dielectric per cubic meter is estimated using the following formula:

$$P_{dielectric} \ (W/m^3) = 2\pi\epsilon f \ E^2 \ tan\delta \qquad (4)$$

where ϵ is the dielectric permittivity, f is the frequency, E is the electric field, and δ is the dielectric loss angle. Since ϵ and $tan\delta$ are constants and E is proportional to V (the applied voltage), equation (4) can be written in the following form:

$$P_{dielectric} \ (W/m^3) = B \ V^2 \ f \qquad (5)$$

where B is a constant, depends on the dielectric material, and can be determined from the relation between the consumed power and the frequency at voltages lower than the onset voltage, where there is no plasma discharge occurs and the total power consumed is the power dissipated in the dielectric material only [39]. To calculate the power at an applied voltage less than the breakdown voltage, the shunt resistor technique is used. This is because the current measured by the resistance was more stable than that measured by the current monitor at an applied voltage less than the breakdown voltage.

The estimated value of B in this reactor at voltages of 1.5 and 2 kV (below the onset voltage) is 2.8×10^{-4} Farad/m^3. This value of B is lower than that in [39], despite a high permittivity of the mica than that for the dielectric materials used in [39]. This can be attributed to the difference in the dimensions of the dielectric material and the electrodes. Using this constant and by assuming that the voltage drop across the discharge is negligible, the dissipated power at any given voltage value higher than the onset voltage can be estimated using equation (5). For example, the estimated values of the dissipated power in the dielectric material at an applied voltage of 5 kV are 7 and 70 mW at frequencies of 1 and 10 kHz, respectively, as shown in table 1. Therefore, the power consumed to generate plasma is 0.20 and 1.95 W at frequencies 1 and 10 kHz, respectively. However, not all of this power value is used to generate reactive species, because the dielectric material receives a part of this power due to the radiation and convection heat transfer between the plasma and the dielectric material, which are expected to depend on the driven frequency.

Figure 7 shows the dependence of the dielectric material temperature on the frequency and the discharge time. As can be seen, the dielectric material temperature increases rapidly with the discharge time after the discharge ignition. The rate of the temperature rise decreases when the discharge time increases before equilibrium establishment at a time of approximately 10 min from the discharge ignition. Moreover, the dielectric material temperature increases with the frequency linearly, as shown in figure 8. From this figure, it can be suggested that the power loss due the heat transfer between the plasma and the dielectric material increases with the frequency linearly. As described above, the discharge

current is high at a higher frequency, which leads to the increase in the collision number of the electrons and ions generated in the plasma filaments with the dielectric material. The higher the frequency of the applied voltage, the higher is the collisions of the electrons and ions with dielectric material. This might explain the increase of the dielectric material temperature with the frequency.
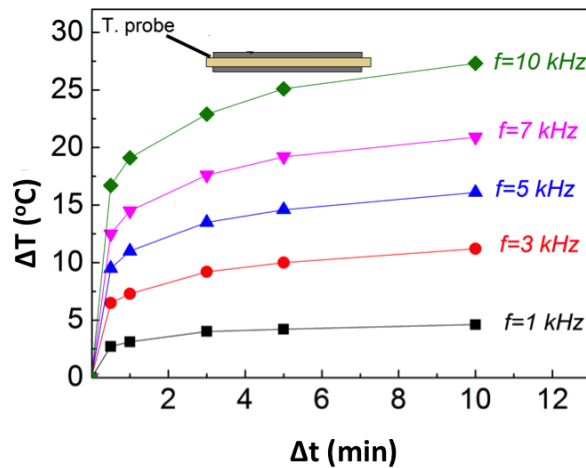

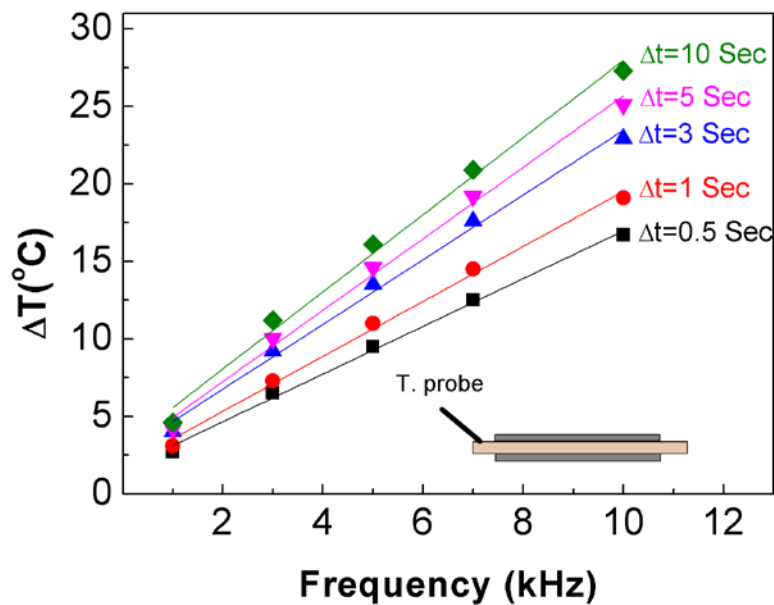**Figure 7** *Dielectric material temperature of the SDBD source at different frequencies.*

Figure 8 *Dielectric material temperature of the SDBD source as a function of the frequency.*

Due to difficulties in determining the transfer coefficient for the convection heat transfer between the plasma and the dielectric material, we could not estimate the convection power lost in the dielectric material. However, by measuring the dielectric material temperature during the discharge, we could calculate the radiation power dissipated in the dielectric

10

material using the Stefan–Boltzmann law as follows:

$$P_{radiation} = e\,\sigma\,S\,(T_t^4 - T_0^4) \qquad (6)$$

where e is the emissivity, σ is the Stefan–Boltzmann constant, S is the surface area of the dielectric material, T_t is the dielectric material temperature after time t of the discharge, and T_0 is the dielectric material temperature before the discharge ignition. Therefore, the radiation power dissipated in the dielectric at a temperature of 5 kV (using 0.8 for the emissivity) is 24.9 and 165.5 mW at frequencies of 1 and 10 kHz, respectively, as shown in table 1. Table 1 indicates that when the frequency is increased the radiation power dissipated in the dielectric material follows a similar trend as the total consumed power and the power dissipated in the dielectric material. The same power should also be consumed during the heat transfer between the plasma and the surrounding gas. Thus, approximately 11.6–15.2 % of the input power dissipates in the dielectric material, and approximately 16.3–23.7 % of the total power is dissipated as heat in the system due to the radiation transfer only. This power loss mainly depends on the nature and dimensions of the dielectric material and on the geometry of the electrodes. Dong et al. [39] used two dielectric materials in their experiment: Teflon and epoxy, and they concluded that the higher the permittivity of the dielectric material, the higher is the dissipated power. It can explain the higher dissipated power obtained in this work than that obtained in [39].

Table 1: Estimation of the discharge and dissipated powers in the SDBD at different frequencies (1–10 kHz) and Vpp = 5 kV

Frequency	Input power	Power dissipated in dielectric	Plasma discharge power	Power dissipated in radiation
(kHz)	(W)	(mW)	(W)	(mW)
1	0.21	7	0.18	24.9
3	0.60	21	0.52	62.2
5	1.00	35	0.87	92.3
7	1.40	49	1.22	122.6
10	2.02	70	1.78	165.5

Optical emission spectroscopy (OES) was used to investigate excited active species generated in the SDBD reactor at different frequencies of 1,5, and 10 kHz and at the same applied peak-to-peak voltage of 6 kV, as shown in figure 9. The fiber probe of an optical emission spectrometer (Ocean optics, USB 2000) was placed outside the reactor, as shown in figure 1, perpendicular to the SDBD source and fixed in front of the plasma generated at a spike of the discharge electrode. A convex lens with a focal length of 50 cm was mounted between the SDBD source and the fiber probe of the spectrometer to focus the emission of the excited species in the SDBD. Figure 9 shows that the main transitions of N-excited species generated in the reactor are the second positive system (SPS) of N_2 $C\,^3\Pi_u - B\,^3\Pi_g$ and the first negative system (FNS) of $N_2^+(B\,^2\Sigma_u^+ - X\,^2\Sigma_g^+)$. Furthermore, the emission intensity of nitrogen-excited species increases with the frequency, which confirms the findings reported in [31, 41]. It

appears that the spectrum peaks increase with the frequency. The intensity of the nitrogen spectrum line at a wavelength of 337 nm increased from 7×10^3 to 34.3×10^3 with the frequency increase from 1 to 5 kHz, respectively, and it increased to 62.4×10^3 at a frequency of 10 kHz. This means that the production rate of nitrogen-excited species at high energy density and frequency decreases slightly. This is probably due to the increase of the dissociation of nitrogen molecules to N atoms at a high energy density, where the cross section of the electronic excitation states of nitrogen decreases exponentially with increasing electron energy [42].
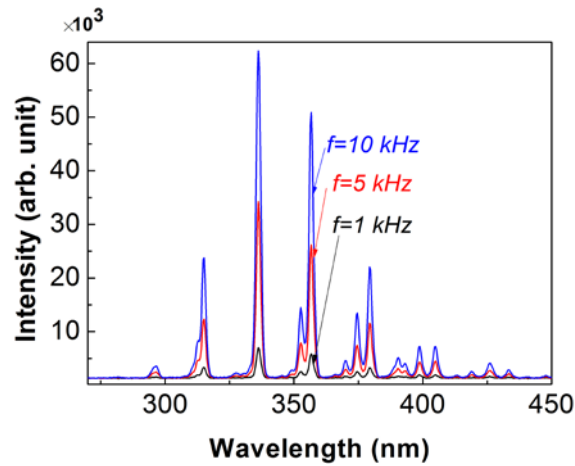

Figure 9 *Optical emission spectra of the SDBD at an applied voltage of 6 kV and different frequencies.*
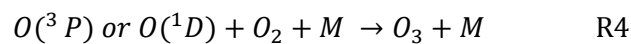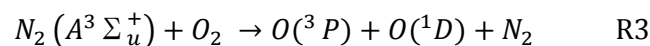
3.3. Ozone production

Ozone formation in plasma discharge starts with the dissociation of an oxygen molecule by the electron impact leading to the generation of a free oxygen atom, which quickly reacts with another oxygen molecule to generate ozone, as described by the following reactions:

$$e + O_2 \rightarrow e + 2O \qquad \text{R1}$$
$$O + O_2 + M \rightarrow O_3 + M \qquad \text{R2}$$
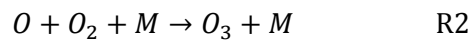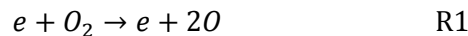
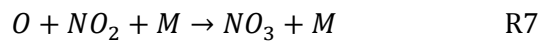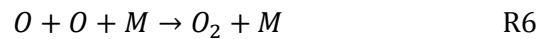where M is the third collision molecule that can be O_2, O_3, or N_2.

In addition, the oxygen-excited species and nitrogen-excited species generated in the plasma discharge play an important role in the generation of oxygen atoms and ozone molecules [43] via the following reactions:

$$N_2\left(A^3 \Sigma_u^+\right) + O_2 \rightarrow O(^3P) + O(^1D) + N_2 \qquad \text{R3}$$

$$O(^3P) \text{ or } O(^1D) + O_2 + M \rightarrow O_3 + M \qquad \text{R4}$$

Ozone molecules formed via the aforementioned processes (R1–R4) are decomposed in the plasma discharge through different processes. The main ozone decomposition processes are as follows:

(1)   A high temperature of the plasma reactor [10], which affects the decomposition of ozone in two ways: (a) thermal decomposition of ozone molecules, and (b) changing the chemical reaction rates that leads to increase the ozone destruction and decrease the ozone production, via the decrease of the reaction rate of reaction R2 [43].
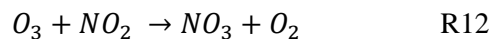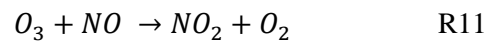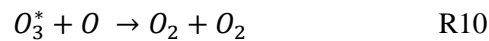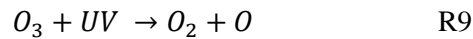
(2)   The temperature of the plasma channels in the reactor, which accelerates the following reactions resulting in ozone decomposition [44].

$$O + O_3 \rightarrow 2O_2 \qquad\qquad \text{R5}$$

$$O + O + M \rightarrow O_2 + M \qquad\qquad \text{R6}$$

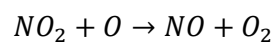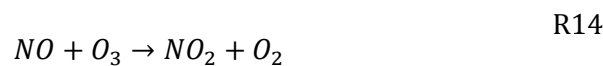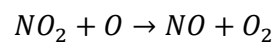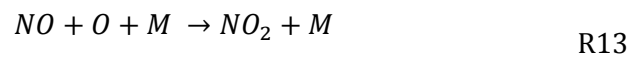$$O + NO_2 + M \rightarrow NO_3 + M \qquad\qquad \text{R7}$$

(3)   The electron impact dissociation of ozone when the electron and ozone concentrations are high in the reactor [44].

$$e + O_3 \rightarrow e + O_2 + O \qquad\qquad \text{R8}$$
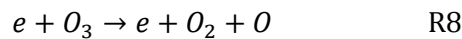
(4)   High UV radiation, oxygen atoms, and nitrogen oxides also contribute to the decomposition of ozone in the reactor at a high input power via the following reactions:

$$O_3 + UV \rightarrow O_2 + O \qquad\qquad \text{R9}$$

$$O_3^* + O \rightarrow O_2 + O_2 \qquad\qquad \text{R10}$$

$$O_3 + NO \rightarrow NO_2 + O_2 \qquad\qquad \text{R11}$$

$$O_3 + NO_2 \rightarrow NO_3 + O_2 \qquad\qquad \text{R12}$$

(5)   The catalytic effect of nitrogen oxides (NO–NO$_2$) in the plasma reactor, which consumes oxygen atoms and destructs ozone via the following two-cycle reactions [45]:

$$NO + O + M \rightarrow NO_2 + M$$
$$\qquad\qquad\qquad\qquad \text{R13}$$
$$NO_2 + O \rightarrow NO + O_2$$

$$\qquad\qquad\qquad\qquad \text{R14}$$
$$NO + O_3 \rightarrow NO_2 + O_2$$

$$NO_2 + O \rightarrow NO + O_2$$

The competition between these decomposition processes of ozone (R5–R14) and its formation processes (R1–R4) depends on various factors, such as the reactor type , operating

parameters, and operation parameters. The dependence of the ozone production on the driven frequency in our reactor is demonstrated in figure 10, where the ozone concentration is shown as a function of the energy density at different frequencies. As can be seen in this figure, the ozone concentration increases with the energy density at all the frequencies. In this work, the maximam ozone concentration obtained is 340 ppm at f = 10 kHz and Vpp = 6 kV, which corresponds to an energy density of 85 J/L.
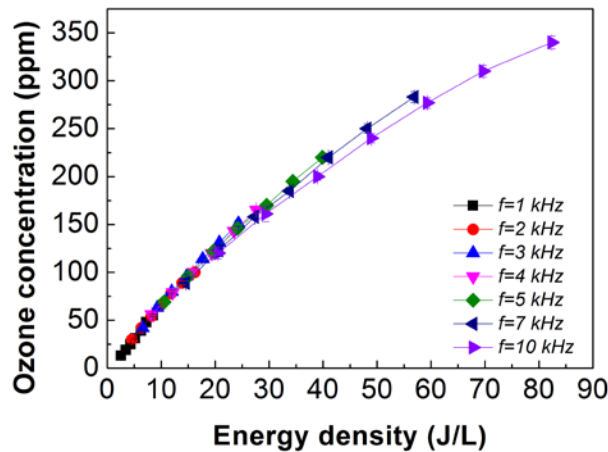

Figure 10 *Ozone concentration as a function of the energy density at different frequencies.*

Figure 10 indicates that the ozone concentration linearly increases with the energy density at low energy densities up to ≈ 10 J/L, and it does not depend on the frequency: the ozone concentration is almost the same for different frequencies at the same energy density (at low energy densities). This result is qualitatively consistent with the work of Simek et al. [34] conducted in the same frequency range. In addition, Shimizu et al. [46] have reported that the ozone concentration in a SDBD-based reactor mainly depends on the input power to the reactor rather than the applied voltage. This can be explained by the independence of the deposited energy in the reactor at one period on the driven frequency, as described above. This is also attributed to the domination of the formation processes of ozone and the negligibility of the decomposition processes at a low energy density [45].

At higher energy densities, the ozone concentration does not increase with the energy density linearly, which is consistent with the ozone concentration obtained in [31, 47, 48]. This indicates the increase of the decomposition processes of ozone (R5–R14) in this energy density range. However, the gas temperature influence can be eliminated due to low temperatures detected in this reactor: 52 $^\circ$C and 39 $^\circ$C at the dielectric material surface and at 1 cm above the dielectric material, respectively. These temperatures are very low to cause ozone thermal decomposition or play a crucial role in the chemical reaction rates. The temperature of the plasma channels might influence the ozone production and the ozone decomposition more significantly than the gas temperature, which is several dozen times lower than that of the plasma channels [44]. Nonetheless, the plasma channels in the SDBD reactor are confined in a small area over the dielectric material and they do not spread in the volume of the reactor. Therefore, the reaction zone around the plasma channels is very small, resulting in an insignificant role of the temperature of the plasma channels in the destruction

14

processes of ozone in our reactor. Therefore, a key process of the decomposition of ozone in our reactor should be the generation of nitrogen oxides and their catalytic effect.

Figure 10 reveals that the ozone concentration decreases when the frequency is increased at the same energy density: the ozone concentration is slightly lower (approximately 10 ppm) at a frequency of 10 kHz than that at a frequency of 5 kHz at the same energy density. Although the difference is not clearly noticeable, it is consistent with the nonlinear behavior of nitrogen-excited species at high frequency and energy density that is described above, where the production rate of nitrogen-excited species is slightly decreased at a frequency of 10 kHz and a high energy density. This finding supports the result reported by Kogelschatz et al. [49] on the effect of the frequency on the generation of nitrogen oxides in a DBD reactor in the frequency range of 100–1600 Hz. This phenomenon implies that the change in the frequency of the applied voltage not only leads to the change in the energy density in the reactor but also might play a role in the kinetic reactions of the generation or decomposition of ozone. This is due to the change of the relaxation time of ions and its effect on the temperature of the discharge channels, which might be influenced by high pulses of the discharge current at a high frequency. Nevertheless, further theoretical and experimental studies are necessary to understand the effect of the frequency on the kinetic reactions of the ozone production.

The dependence of the energy yield of the ozone production on the frequency as a function of the energy density is depicted in figure 11. As can be observed, the energy yield initially increases with the energy density and reaches a maximum at an energy density of approximately of 10 J/L. A similar behavior was obtained by Pemen et al. [50] in a wire-to-plate corona reactor, where the energy yield of the ozone production linearly increased with the energy density at energy density values lower than 13 J/L. A further increase in the energy density, larger than 10 J/L, caused a subsequent sharp decrease in the energy yield of the ozone production regardless of the driven frequency. After the maximum of the energy yield, the energy yield decreases as the frequency increases at the same energy density. This result is consistent with that obtained by Masuda et al. [19], where the ozone production decreased sharply at a certain applied voltage at frequencies of 7 and 10 kHz. The increase of the energy yield with the energy density up to 10 J/L confirms that the formation process of ozone is dominant and the decomposition process of ozone is almost negligible in this range of energy density. On the other hand, the decrease of the energy yield of ozone after an energy density of 10 J/L indicates that the deposited energy is not used in the reactor effectively for generating ozone, but it consumed in the formation of unfavorable species (via I.2 in figure 6), which resulting in the decrease in the energy yield of the ozone production.

The highest energy yield achieved in our reactor is approximately 52 g/kWh (corresponds to the ozone concentration of 50 ppm) at an energy density of 10 J/L and at frequencies of 3 and 4 kHz. This result indicates that the energy is consumed in the SDBD reactor more efficiently for the ozone production, when it is operated at low frequencies and the energy density is less than 10 J/L (i.e., the dominant part of the consumed energy is used to generate ozone via I.1, as shown in figure 6, rather than produce unfavorable species or heat the system).
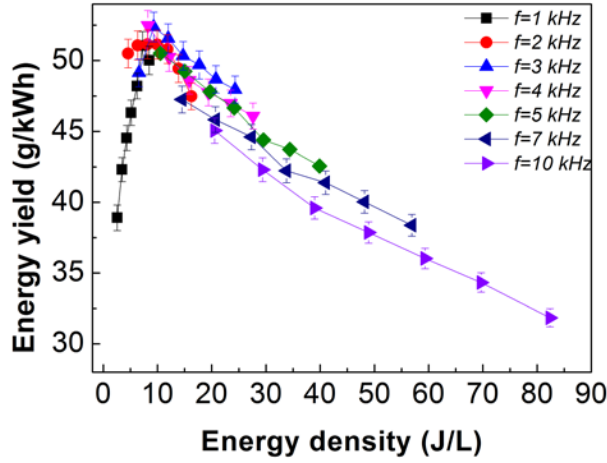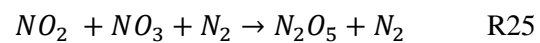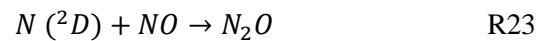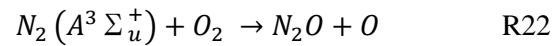
Figure 11 *Energy yield of the ozone production as a function of the energy density at different frequencies.*

3.4. Nitrogen byproducts

In this work, Fourier transform absorption spectroscopy is used to identify the gaseous byproducts associated with the ozone production as well as to quantify the concentrations of nitrogen oxide byproducts in the reactor. These compounds are generated by the following reactions of nitrogen molecules or atoms with oxygen atoms or molecules [51–54]:

$$N_2 \left(A^3 \Sigma_u^+ \right) + O \rightarrow NO + N \left(^2D \right) \qquad \text{R15}$$

$$N \left(^2D \right) + O_2 \rightarrow NO + O(^3P) \qquad \text{R16}$$

$$N \left(^2P \right) + O_2 \rightarrow NO + O \qquad \text{R17}$$

$$O + NO \rightarrow NO_2 \qquad \text{R18}$$

$$O + NO_2 \rightarrow NO + O_2 \qquad \text{R19}$$

$$O + NO_2 \rightarrow NO_3 \qquad \text{R20}$$

$$O \left(^3P \right) + NO_2 + N_2 \rightarrow NO_3 + N_2 \qquad \text{R21}$$

$$N_2 \left(A^3 \Sigma_u^+ \right) + O_2 \rightarrow N_2O + O \qquad \text{R22}$$
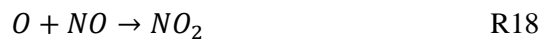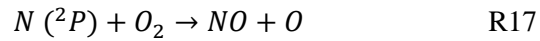
$$N \left(^2D \right) + NO \rightarrow N_2O \qquad \text{R23}$$

$$N + NO \rightarrow N_2O \qquad \text{R24}$$

$$NO_2 + NO_3 + N_2 \rightarrow N_2O_5 + N_2 \qquad \text{R25}$$
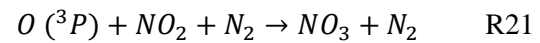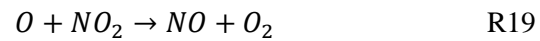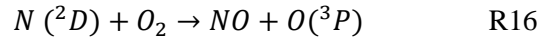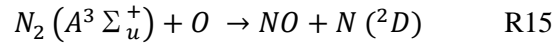
Therefore, these measurements can clarify the dependence of the production efficiency of ozone in this reactor on the frequency. The emission of these compounds into the atmosphere

16

has a significant adverse effect on the environment and on human health. Since these compounds are considered as strong oxidizing agents, they react in air forming corrosive nitric acid and toxic organic nitrates. In water treatment using ozone generated by plasma discharge, these compounds play a key role in the decrease in the pH of the water [22], which affects the reactor performance to decompose pollutants [55].

Figure 12 shows typical FTIR spectra of the gas byproducts generated during the ozone production in the SDBD reactor at Vpp = 6 kV and different frequencies of 1, 3, , 5, and 10 kHz) in dry air. The main byproducts found in the spectra are N_2O, N_2O_5, and NO_2, which are similar to those obtained in [56]. The qualitative FTIR spectrometry measurements show that ozone is the dominant reactive species generated in the reactor at all the frequencies. Moreover, the peaks of the nitrogen oxide species in the FTIR spectra show that N_2O_5 is the dominant nitrogen oxide species generated in the reactor, and it is the second dominant reactive species after ozone. Figure 12 also reveals that the peaks of ozone and the peaks of all the byproducts increase with the driven frequency. This is due to the increase of the energy density of the SDBD reactor with the frequency, as described above, and thus, increases the energy and/or the density of the electrons that induce high reactive species in the reactor to produce these byproducts. By contrast, Olszewski et al. [25] found that the O_3 concentration decreased when the input power to the SDBD reactor was increased despite the increase of the concentrations of all the nitrogen oxides in the reactor. The difference between the ozone concentration with respect to the power obtained in our case and that obtained in [25] can be attributed to elevated temperatures associated with high-power operation used in their reactor.

The absence of NO in the spectra can be due to its easy oxidation to NO_2 (R11 and R18) [49, 54, 57] and its oxidation via NO_2 and NO_3 to another oxidation state N_2O_5 (R25) [52].
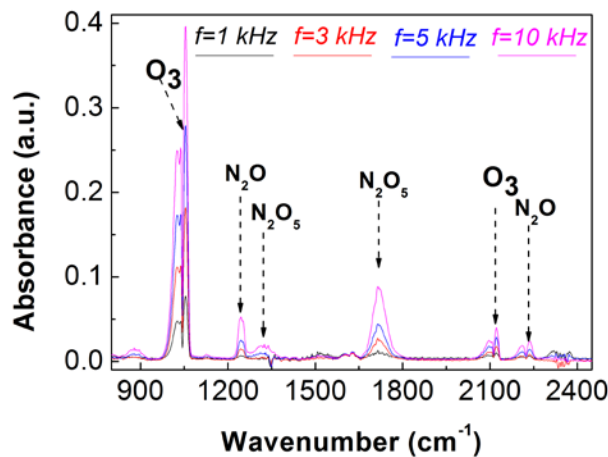
Figure 12 *FTIR spectra at different frequencies and constant applied voltage V*pp = 6 kV.

Figure 13 shows the concentration of N_2O as a function of the energy density at different frequencies. The N_2O concentration is linearly increased with the energy density in the SDBD reactor regardless of the driven frequency. The same behavior is obtained in [34, 53]. The highest N_2O concentration is approximately 6.9 ppm at an energy density of 85 J/L and a frequency of 10 kHz. At a low energy density (10 J/L), the concentration of N_2O is very low (approximately 1 ppm) due to low reactive species, such as $N_2\left(A^3 \Sigma_u^+\right)$, $N\left(^2D\right)$, and O, that

lead to the N_2O formation via reactions R10, R17, and R18. In addition, the energy of electrons in the reactor is probably increased with the energy density, which leads to the increase in the nitrogen atom concentrations to the detriment of generating nitrogen-excited species. This result can also explain the decrease of the energy yield of the ozone production in figure 11 at energy density values larger than 10 J/L.
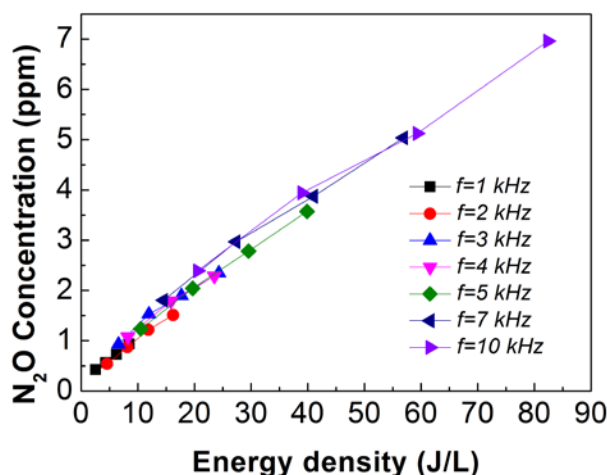

Figure 13 *N_2O production in the SDBD reactor as a function of the energy density at different frequencies.*

Figure 14 shows the concentration of NO_2 as a function of the energy density at different frequencies. As can be observed in the figure, the concentration of NO_2 is very low in the reactor, and the maximum NO_2 concentration is 2.3 ppm at an energy density of 30 J/L and a frequency of 5 kHz. Therefore, the peak of NO_2 does not appear in the FTIR spectra (figure 12). This can be due to the conversion of NO_2 to a higher oxidation state N_2O_5, either directly via reaction R25 or indirectly through its oxidation via reaction R21 followed by reaction R25. This can explain the higher concentration of N_2O_5 that observed in the FTIR spectra. At low frequency and energy density values, the concentration of NO_2 increases with the energy density. The behavior of the NO_2 concentration is almost linear with respect to the energy density at low energy density values, which is consistent with the result obtained by Guo et al. [54] in a DBD-based reactor despite a high energy density used in their work. The linear behavior of the NO_2 concentration with respect to the energy density at low energy densities (less than 15 J/L) indicates a constant yield of NO_2, It can explain the increase of the energy yield of the ozone production in this range of the energy density. However, the linear behavior of the NO_2 concentration is changed when the energy density and the frequency are increased. Moreover, at a higher constant energy density (greater than 20 J/L), the NO_2 concentration decreases as the frequency is increased. A phenomenon similar to this has also been seen by Kogelschatz et al. [49] in the frequency range of 200–1600 Hz. This result supports the aforementioned assumption regarding the effect of the frequency on the kinetic reactions due to the increase of the collision of electrons and ions with molecules.

Low concentrations of NO and NO_2 simultaneously with relatively high concentrations of N_2O and N_2O_5 implies that the oxidation of NO and NO_2 to another nitrogen oxides (N_2O and

N$_2$O$_5$) in this reactor plays an important role in the decrease of the ozone concentration, especially at a high concentration of ozone as found in [58]. Although the N$_2$O$_5$ concentration is not determined quantitatively (due to the unavailability of N$_2$O$_5$ mixtures of the certified concentrations on the market), the FTIR spectra indicate a high concentration of N$_2$O$_5$ in the reactor at high frequency and energy density.
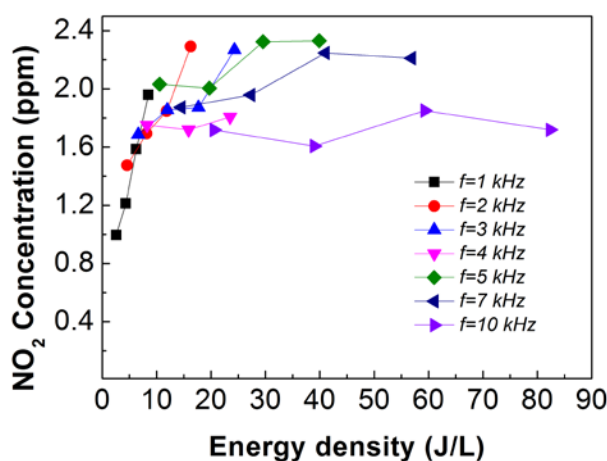

Figure 14 *NO$_2$ production in the SDBD reactor as a function of the energy density at different frequencies.*

4. Conclusions

An experimental study on the influence of the frequency of the applied voltage on the electrical characterization of SDBD is carried out to evaluate the ozone production using SDBD. In addition, the nitrogen oxide concentrations are evaluated at different frequencies to evaluate the performance of an SDBD reactor in the ozone production. The main results of this study can be summarized as follows:

(1) SDBD is operated in the filamentary mode in the frequency range of 1–10 kHz. However, at one cycle of the applied voltage, the pulses of the discharge current are much denser and have higher amplitudes at a high frequency than those at a low frequency. Nevertheless, the energy density increases with the frequency linearly.

(2) The analysis of the power consumed in the reactor clarifies the distribution of the input power in the reactor and its impact on the efficiency of the reactor to produce reactive species, e.g., ozone. A small portion of the energy consumed by the SDBD reactor is absorbed in the dielectric material, while a significant part is used to generate plasma discharge. Not all the plasma energy is used to generate reactive species for the ozone production: its significant part is dissipated as heat in the system.

(3) The maximum temperatures measured in the reactor are 52 $^{\circ}$C at the dielectric material surface and 39 $^{\circ}$C at 1 cm above its surface. These temperatures are insufficient for thermal decomposition of ozone in the reactor.

19

(4) The ozone concentration linearly increases with the energy density at low values regardless of the frequency. The results also indicate that the energy is consumed in the SDBD more efficiently for the ozone production when it is operated at low frequencies, where the energy yield linearly increases with the energy density up to 10 J/L. Moreover, the frequency has a slightly adverse effect on the ozone concentration at high energy densities.

(5) The highest energy yield achieved in the SDBD reactor is approximately 52 g/kWh at an energy density of 10 J/L. The increase in the energy density above 10 J/L causes a sharp decrease in the energy yield of the ozone production regardless of the driven frequency.

(6) The concentrations of NO and NO_2 are very low in the reactor, whereas N_2O_5 is the dominant nitrogen oxide found in the reactor due to the oxidation of NO and NO_2 to N_2O_5. Therefore, the formation of NO and NO_2 in the reactor plays a key role in the decomposition of ozone due to their oxidation to another oxide species and their catalytic effect.

References

[1]   A. Mizuno, "Industrial applications of atmospheric non-thermal plasma in environmental remediation," *Plasma Physics and Controlled Fusion,* vol. 49, pp. A1-A15, 2007.

[2]   G. Fridman, G. Friedman, A. Gutsol, A. B. Shekhter, V. N. Vasilets, and A. Fridman, "Applied Plasma Medicine," *Plasma Processes and Polymers,* vol. 5, pp. 503-533, 2008.

[3]   S. Samukawa, M. Hori, S. Rauf, K. Tachibana, P. Bruggeman, G. Kroesen*, et al.,* "The 2012 Plasma Roadmap," *Journal of Physics D: Applied Physics,* vol. 45, p. 253001, 2012.

[4]   M. G. Kong, G. Kroesen, G. Morfill, T. Nosenko, T. Shimizu, J. van Dijk*, et al.,* "Plasma medicine: an introductory review," *New Journal of Physics,* vol. 11, p. 115012, 2009.

[5]   N. Benard and E. Moreau, "Electrical and mechanical characteristics of surface AC dielectric barrier discharge plasma actuators applied to airflow control," *Experiments in Fluids,* vol. 55, 2014.

[6]   Y. Hozumi, T. Seto, M. Hirasawa, M. Tsuji, and A. Okuyama, "Kinetics of microplasma atmospheric ion generation correlated with discharge current," *Journal of Electrostatics.,* vol. 67, pp. 1-6, 2009.

[7]   E. Manirakiza, T. Seto, S. Osone, K. Fukumori, and Y. Otani, "High-Efficiency Unipolar Charger for Sub-10 nm Aerosol Particles Using Surface-Discharge Microplasma with a Voltage of Sinc Function," *Aerosol Science and Technology,* vol. 47, pp. 60-68, 2013/01/01 2012.

[8]   M. A. Malik, "Ozone Synthesis Using Shielded Sliding Discharge- Effect of Oxygen Content and Positive versus Negative Streamer Mode," I*ndustrial & Engineering Chemistry Research,* vol. 53, pp. 12305-12311, 2014.

[9]   M. A. Malik, D. Hughes, R. Heller, and K. H. Schoenbach, "Surface Plasmas Versus Volume Plasma: Energy Deposition and Ozone Generation in Air and Oxygen," *Plasma Chemistry and Plasma Processing,* vol. 35, pp. 697-704, 2015.

[10]   S. Jodzis, Smolin, x, T. ski, So, x*, et al.,* "Ozone Synthesis Under Surface Discharges in Oxygen: Application of a Concentric Actuator,"*, IEEE Transactions on Plasma Science,* vol. 39, pp. 1055-1060, 2011.

[11]   M. A. Malik, K. H. Schoenbach, and R. Heller, "Coupled surface dielectric barrier discharge reactor-ozone synthesis and nitric oxide conversion from air," *Chemical Engineering journal,* vol. 256, pp. 222-229, 2014.

[12]   A. Abdelaziz, T. Seto, M. Abdel-Salam, and Y. Otani, "Influence of N2/O2 Mixtures on Decomposition of Naphthalene in Surface Dielectric Barrier Discharge Based Reactor," *Plasma Chemistry and Plasma Processing,* vol. 34, pp. 1371-1385, 2014/11/01 2014.

[13]   T. Seto, S. B. Kwon, M. Hirasawa, and A. Yabe, "Decomposition of Toluene with Surface-Discharge Microplasma Device," *Japanese Journal of Applied Physics,* vol. 44, pp. 5206-5210, 2005.

[14]   J. Jeon, T. G. Klaempfl, J. L. Zimmermann, G. E. Morfill, and T. Shimizu, "Sporicidal properties from surface micro-discharge plasma under different plasma conditions at different humidities," *New Journal of Physics,* vol. 16, p. 103007, 2014.

[15]   T. Maisch, T. Shimizu, Y. F. Li, J. Heinlin, S. Karrer, G. Morfill*, et al.,* "Decolonisation of MRSA, S. aureus and E. coli by cold-atmospheric plasma using a porcine skin model in vitro," *PLoS One,* vol. 7, p. e34610, 2012.

[16]   G. E. Morfill, T. Shimizu, B. Steffes, and H. U. Schmidt, "Nosocomial infections—a new approach towards preventive medicine using plasmas," *New Journal of Physics,* vol. 11, p. 115019, 2009.

[17]   J. Jeon, T. M. Rosentreter, Y. Li, G. Isbary, H. M. Thomas, J. L. Zimmermann*, et al.,* "Bactericidal Agents Produced by Surface Micro-Discharge (SMD) Plasma by

Controlling Gas Compositions," *Plasma Processes and Polymers,* vol. 11, pp. 426-436, 2014.

[18]   K. Shimizu, M. Yamada, M. Kanamori, and M. Blajan, "Basic Study of Bacteria Inactivation at Low Discharge Voltage by Using Microplasmas," *IEEE transactions on industry applications,* vol. 46, pp. 641-649, 2010.

[19]   S. Masuda, K. Akutsu, M. Kuroda, Y. Awatsu, and Y. Shibuya, "A Ceramic-Based Ozonizer Using High-Frequency Discharge," *IEEE transactions on industry applications,* vol. 24, pp. 223-232, 1988.

[20]   M. A. Malik, J. F. Kolb, Y. Sun, and K. H. Schoenbach, "Comparative study of NO removal in surface-plasma and volume-plasma reactors based on pulsed corona discharges," *Journal of Hazardous Materials,* vol. 197, pp. 220-8, Dec 15 2011.

[21]   M. J. Pavlovich, D. S. Clark, and D. B. Graves, "Quantification of air plasma chemistry for surface disinfection," *plasma sources science and Technolgy,* vol. 23, pp. 065036-065046, 2014.

[22]   K. Oehmigen, M. Hähnel, R. Brandenburg, C. Wilke, K. D. Weltmann, and T. von Woedtke, "The Role of Acidification for Antimicrobial Activity of Atmospheric Pressure Plasma in Liquids," *Plasma Processes and Polymers,* vol. 7, pp. 250-257, 2010.

[23]   K. Shimizu, S. Muramatsu, T. Sonoda, and M. Blajan, "Water Treatment by Low Voltage Discharge in Water," *International Journal of Plasma Environmental Science & Technology,* vol. 4, pp. 58-64, 2010.

[24]   K. Shimizu, N. Masamura, and M. Blajan, "Water Purification by Using Microplasma Treatment," *Journal of Physics: Conference Series,* vol. 441, p. 012005, 2013.

[25]   P. Olszewski, J. F. Li, D. X. Liu, and J. L. Walsh, "Optimizing the electrical excitation of an atmospheric pressure plasma advanced oxidation process," *Journal of Hazardous Materials,* vol. 279, pp. 60-6, Aug 30 2014.

[26]   S. Li, X. Ma, Y. Jiang, and X. Cao, "Acetamiprid removal in wastewater by the low-temperature plasma using dielectric barrier discharge," *Ecotoxicology Environmental Safety,* vol. 106, pp. 146-53, Aug 2014.

[27]   C. W. Chen, H. M. Lee, and M. B. Chang, "Inactivation of Aquatic Microorganisms by Low-Frequency AC Discharges," *IEEE transactions on plasma science,* vol. 36, pp. 215-219, 2008.

[28]   D. B. Graves, "The emerging role of reactive oxygen and nitrogen species in redox biology and some implications for plasma applications to medicine and biology," *Journal of Physics D: Applied Physics,* vol. 45, p. 263001, 2012.

[29]   W. Tian and M. J. Kushner, "Atmospheric pressure dielectric barrier discharges interacting with liquid covered tissue," *Journal of Physics D: Applied Physics,* vol. 47, p. 165201, 2014.

[30] S. Pekárek, "Experimental study of surface dielectric barrier discharge in air and its ozone production," *Journal of Physics D: Applied Physics,* vol. 45, p. 075201, 2012.

[31] S. Pekárek, "Asymmetric properties and ozone production of surface dielectric barrier discharge with different electrode configurations," *The European Physical Journal D,* vol. 67:94, pp. 1-7, 2013.

[32] N. Mastanaiah, P. Banerjee, J. A. Johnson, and S. Roy, "Examining the Role of Ozone in Surface Plasma Sterilization Using Dielectric Barrier Discharge (DBD) Plasma," *Plasma Processes and Polymers,* vol. 10, pp. 1120-1133, 2013.

[33] M. Simek, S. Pekarek, and V. Prukner, "Ozone Production Using a Power Modulated Surface Dielectric Barrier Discharge in Dry Synthetic Air," *Plasma Chemistry and Plasma Processes,* vol. 32, pp. 743-754, 2012.

[34] M. J. Pavlovich, H.-W. Chang, Y. Sakiyama, D. S. Clark, and D. B. Graves, "Ozone correlates with antibacterial effects from indirect air dielectric barrier discharge treatment of water," *Journal of Physics D: Applied Physics,* vol. 46, p. 145202, 2013.

[35] D. Hong, H. Rabat, J. M. Bauchire, and M. B. Chang, "Measurement of Ozone Production in Non-thermal Plasma Actuator Using Surface Dielectric Barrier Discharge," *Plasma Chemistry and Plasma Processes,* vol. 34, pp. 887-897, 2014.

[36] A. Abdelaziz, T. Seto, M. Abdel-Salam, and Y. Otani, "Performance of a surface dielectric barrier discharge based reactor for destruction of naphthalene in an air stream," *Journal of Physics D: Applied Physics,* vol. 45, p. 115201, 2012.

[37] M. Forte, J. Jolibois, J. Pons, E. Moreau, G. Touchard, and M. Cazalens, "Optimization of a dielectric barrier discharge actuator by stationary and non-stationary measurements of the induced flow velocity: application to airflow control," *Experiments in Fluids,* vol. 43, pp. 917-928, 2007.

[38] M. Kotsonis, "Diagnostics for characterisation of plasma actuators," *Measurement Science and Technology,* vol. 26, p. 092001, 2015.

[39] B. Dong, J. M. Bauchire, J. M. Pouvesle, P. Magnier, and D. Hong, "Experimental study of a DBD surface discharge for the active control of subsonic airflow," *Journal of Physics D: Applied Physics,* vol. 41, p. 155201, 2008.

[40] J. P. Boeuf, Y. Lagmich, T. Unfer, T. Callegari, and L. C. Pitchford, "Electrohydrodynamic force in dielectric barrier discharge plasma actuators," *Journal of Physics D: Applied Physics,* vol. 40, pp. 652-662, 2007.

[41] H. Wedaa, Abdel-Salam, A. Ahmed, and A. Mizuno, "NO Removal Using Dielectric Barrier Discharges in a Multi- rod Reactor Stressed by AC and Pulsed High Voltages," *IEEE Transaction on Dielectrics and Electrical Insulation,* vol. 18, pp. 1743-1751, 2011.

[42] Y. Itikawa, "Cross Sections for Electron Collisions with Nitrogen Molecules," *Journal of Physical and Chemical Reference Data,* vol. 35, pp. 31-53, 2006.

[43] J. Chen and J. H. Davidson, "Ozone Production in the Positive DC Corona Discharge- Model and Comparison to Experiments," *Plasma Chemistry and Plasma Processing,* vol. 22, pp. 495-522, 2002.

[44] S. Jodzis, "Application of Technical Kinetics for Macroscopic Analysis of Ozone Synthesis Process," *Industrial & Engineering Chemistry Research,* vol. 50, pp. 6053-6060, 2011.

[45] A. Yehia, "Assessment of ozone generation in dry air fed silent discharge reactors," *Physics of Plasmas,* vol. 19, p. 023503, 2012.

[46] T. Shimizu, Y. Sakiyama, D. B. Graves, J. L. Zimmermann, and G. E. Morfill, "The dynamics of ozone generation and mode transition in air surface micro-discharge plasma at atmospheric pressure," *New Journal of Physics,* vol. 14, p. 103028, 2012.

[47] S. Jodzis, "Effect of Silica Packing on Ozone Synthesis from Oxygen-Nitrogen Mixtures," *Ozone: science & Engineering,* vol. 25, pp. 63-72, 2002.

[48] S. Yagi and M. Tanaka, "Mechanism of ozone generation in air-fed ozonisers," *Journal of Physics D: Applied Physics,* vol. 12, pp. 1509-1522, 1979.

[49] U. Kogelschatz and P. Baessler, "Determination of Nitrous Oxide and Dinitrogen Pentoxide Concentrations in the Output of Air-Fed Ozone Generators of High Power Density," *Ozone: Science & Engineering,* vol. 9, pp. 195-206, 1987.

[50] A. J. M. Pemen, T. H. P. Ariaans, L. Zhen, E. J. M. Heesch, G. J. J. Winands, and Y. Keping, "AC/DC power modulation for corona plasma generation," in *11th International conference on electrostatic precipitation*, Hangzhou, 2008, pp. 629-632.

[51] S. Sakai, M. Matsuda, D. Wang, T. Namihira, H. Akiyama, K. Okamoto, *et al.*, "Nitric Oxide Generator Based on Pulsed Arc Discharge," *Acta Physics Polonica A,* vol. 115, pp. 1104-1106, 2009.

[52] U. Kogelschatz, B. Eliasson, and M. Hirth, "Ozone generation from oxygen and air- discharge physics and reaction mechanisms," *Ozone science & Engineering,* vol. 10, pp. 367-378, 1988.

[53] S. Lovascio, N. Blin-Simiand, L. Magne, F. Jorand, and S. Pasquiers, "Experimental Study and Kinetic Modeling for Ethanol Treatment by Air Dielectric Barrier Discharges," *Plasma Chemistry and Plasma Processing,* vol. 35, pp. 279-301, 2014.

[54] Y. Guo, X. Liao, M. Fu, H. Huang, and D. Ye, "Toluene decomposition performance and NOx by-product formation during a DBD-catalyst process," *Journal of Environtal Science,* vol. 28, pp. 187-94, Feb 1 2015.

[55] S. Ikawa, K. Kitano, and S. Hamaguchi, "Effects of pH on Bacterial Inactivation in Aqueous Solutions due to Low-Temperature Atmospheric Pressure Plasma Application," *Plasma Processes and Polymers,* vol. 7, pp. 33-42, 2010.

[56] K. Hensel, Z. Machala, and P. Tardiveau, "Capillary microplasmas for ozone generation," The *European Physical Journal Applied Physics,* vol. 47, pp. 22813-22818, 2009.

[57] V. Cooray and M. Rahman, "Efficiencies for production of NOx and O3 by streamer discharges in air at atmospheric pressure," *Journal of Electrostatics,* vol. 63, pp. 977-983, 2005.

[58] K. Skalska, J. Miller, and S. Ledaowicz, "NO removal from flue gases by ozonation," *Environment protection engineering,* vol. 35, pp. 207-214, 2009.